CHEMISTRY
A EUROPEAN JOURNAL

FULL PAPER

DOI: 10.1002/chem.201200547

Silver-Catalysed Enantioselective Addition of O–H and N–H Bonds to Allenes: A New Model for Stereoselectivity Based on Noncovalent Interactions

Jannine L. Arbour,[a] Henry S. Rzepa,[a] Julia Contreras-García,*[b] Luis A. Adrio,[a] Elena M. Barreiro,[a] and King Kuok (Mimi) Hii*[a]

Abstract: The ability of silver complexes to catalyse the enantioselective addition of O–H and N–H bonds to allenes is demonstrated for the first time by using optically active anionic ligands that were derived from oxophosphorus(V) acids as the sources of chirality. The intramolecular addition of acids, alcohols, and amines to allenes can be achieved with up to 73% *ee*. The exploitation of a C–H anomeric effect allowed the absolute configuration of a sample of 2-substituted tetrahydrofuran of low *ee* to be unambiguously assigned by comparison of the chiroptical ORD and VCD measurements with calculated spectra. In the second part of the work, the origin of the stereoselectivity was probed by DFT free-energy calculations of the transition states. A new model of enantiomeric differentiation was developed that was based on noncovalent interactions. This model allowed us to identify the source of stereoselectivity as weak attractive interactions; such dispersive forces are often overlooked in asymmetric catalysis. A new computational approach was developed that represents these interactions as colour-coded isosurfaces that are characterised by the reduced density-gradient profile.

Keywords: allenes · asymmetric catalysis · computational chemistry · noncovalent interactions · stereoselectivity

Introduction

Many metal complexes have been reported to catalyse the addition of O–H and N–H bonds to allenes, but enantioselective examples of such transformations are rare.[1,2] In this regard, the discovery of cationic gold(I) complexes as enantioselective catalysts for these reactions is particularly significant, because excellent levels of stereoselectivity can be attained by using optically active diphosphine ligands and/or counterions.[3] More recently, the use of chiral Brønsted acids for enantioselective intramolecular N–H additions to 1,2- and 1,3-dienes was also reported, but those reactions were comparatively sluggish (required 10 mol% catalyst loading and 48 h).[4]

In our earlier study on the Ag-catalysed cyclisation of γ-allenols,[5] certain counteranions ($CF_3SO_3^-$ and $CF_3CO_2^-$) were found to be intimately involved in the stereodefining transition states, which also exerted significant influence on the reaction rate. This observation led us to postulate that asymmetric catalysis may be feasible by employing optically active anions. Subsequently, a study was performed with a number of silver salts of chiral acids (see the Supporting Information, Table S1). Herein, we report that notable enantioselectivity can be obtained by using oxophosphorus(V) acids **1-H** and **2-H** (Scheme 1, Figure 1). As far as we are aware, this is the first time that chiral silver complexes has been shown to facilitate the enantioselective additions of O–H and N–H bonds to prochiral allenes as a catalyst.[6,7]

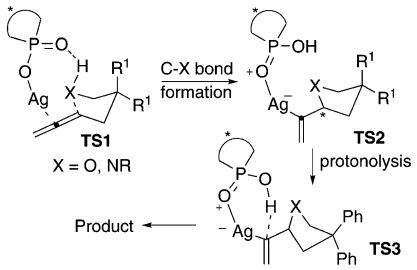

Scheme 1. Sequential C–X and C–H bond-forming processes.

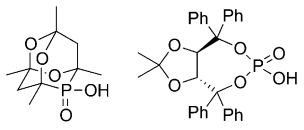

Figure 1. Chiral oxophosphorus(V) acids used in this work.

[a] Dr. J. L. Arbour, Prof. H. S. Rzepa, Dr. L. A. Adrio, Dr. E. M. Barreiro, Prof. K. K. Hii
Department of Chemistry, Imperial College London
Exhibition Road, South Kensington, London SW7 2AZ (UK)
E-mail: mimi.hii@imperial.ac.uk

[b] Dr. J. Contreras-García
Laboratoire de Chimie Théorique
Université Pierre et Marie Curie, 75005 Paris (France)
E-mail: julia.contreras66@gmail.com

Supporting information for this article is available on the WWW under http://dx.doi.org/10.1002/chem.201200547.

During the course of this study, DFT calculations were employed for the stereochemical assignment of the cyclised products by comparison of their chiroptical properties with predicted values. Finally, a new computational model was developed to reveal the origin of the stereoselectivity, which may be attributed to weakly attractive noncovalent interactions between the ligand and the substrate in the transition-state structures.

Results and Discussion

Silver(I) complexes **1-Ag** and **2-Ag** were prepared from the reactions of Ag_2CO_3 with β-CgPOOH (**1-H**)[8,9] and TADDOL-POOH (**2-H**),[10] respectively. These complexes, which were isolated as white solids and were soluble in most organic solvents, were fully characterised. Elemental analysis revealed a metal-to-ligand ratio of 1:1 and the observation of oligomeric mass ions ($[nM]^+$, where $n=1, 2, 3$) in the MS (ESI) spectra suggested that they likely existed as aggregates/polymers. By using 2,2-diphenyl-substituted γ-allenol (**3a**) as a model substrate, the catalytic activity of these silver complexes was initially assessed in DCE under different reaction conditions (Scheme 2, Table 1).

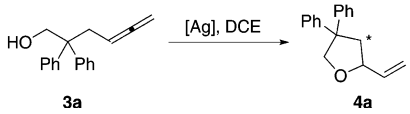

Scheme 2. Cyclisation of model substrate **3a**.

Table 1. Cyclisation of compound **3a** in the presence of silver catalysts.[a]

Entry	[Ag] (mol%)	T [°C]	t [h]	Conversion [%][b]	e.r.[c]
1	**1-Ag** (15)	23	0.5	100	36:64
2	**2-Ag** (15)	23	8	100	41:59
3	**1-Ag** (5)	23	2	100	36:64
4	**1-Ag** (2.5)	23	7	100	36:64
5	**1-Ag** (15)	0	4	100	33.5:66.5
6	**1-Ag** (15)	−10	17	100	33.5:66.5
7	**1-H** (15)	23	168	–	–
8	**2-H** (15)	23	168	–	–

[a] Reaction conditions: Compound **3a** (0.1 mmol), catalyst, DCE (0.5 mL); [b] Determined by ^{1}H NMR spectroscopy. [c] Determined by chiral HPLC. The *S*-enantiomer predominated in all cases.

The reaction that is catalysed by phosphinate salt **1-Ag** is faster than that mediated by phosphate **2-Ag** (Table 1, entries 1 and 2), thereby confirming the effect of the counteranion on the rate-determining step. As a consequence, the reactions that are catalysed by compound **1-Ag** can be performed at lower catalytic loading (Table 1, entries 3 and 4) or temperature (Table 1, entries 5 and 6) without any adverse effects. For substrate **3a**, compound **1-Ag** is slightly more selective (33% *ee*) than compound **2-Ag** (28% *ee*), with the formation of the *S*-enantiomer being favoured in both cases. Last but not least, the operation of chiral Brønsted acid catalysis can be categorically excluded from control experiments (Table 1, entries 7 and 8).[4a,11,12]

Subsequently, the cyclisation reactions of a series of allenols and allenoic acids was performed under the optimised conditions by using 5 and 15 mol% of compounds **1-Ag** and **2-Ag**, respectively (Scheme 3, Table 2). Overall, the reactions that are catalysed by compound **2-Ag** appear to be

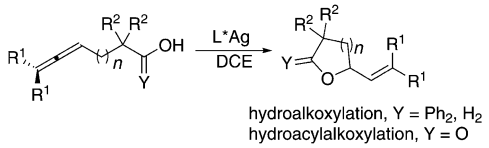

Scheme 3. Intramolecular cyclisation of allenols and allenoic acids.

Table 2. Ag-catalysed hydro(acy)alkoxylation reactions.[a]

Entry	Product	L*Ag	t [h]	Yield [%][b]	e.r.[c]
1	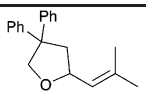	**1-Ag** (5)	2	97	33:67[d]
2		**2-Ag** (15)	8	98	32:68[d]
	4b				
3	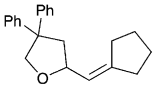	**1-Ag** (5)	2	99	42:58
4		**2-Ag** (15)	8	98	29.5:70.5
	4c				
5	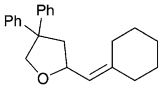	**1-Ag** (5)	2	96	16.5:83.5[d]
6		**2-Ag** (15)	8	99	13.5:86.5[d]
	4d				
7	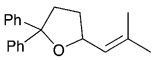	**1-Ag** (5)	15	95	28.5:71.5
8		**2-Ag** (15)	168	33[e]	33:67
	4e				
9	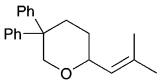	**1-Ag** (5)	5	98	41:59[d]
10		**2-Ag** (15)	12	91	56:44
	4f				
11	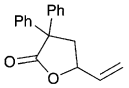	**1-Ag** (5)	2	99	54:46
12		**2-Ag** (15)	3	97	38.5:61.5
	5a				
13	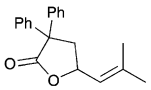	**1-Ag** (5)	2	96	59:41
14		**2-Ag** (15)	3	98	46.5:53.5
	5b				
15	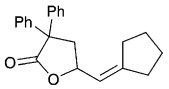	**1-Ag** (5)	2	98	57.5:42.5
16		**2-Ag** (15)	3	96	48:52
	5c				
17	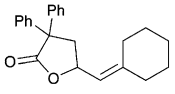	**1-Ag** (5)	2	98	62:38
18		**2-Ag** (15)	3	98	42.5:57.5
	5d				

[a] Reaction conditions: Substrate (0.1 mmol), DCE (0.5 mL), 23°C; [b] yield of isolated product after purification by column chromatography on silica gel. [c] Determined by chiral HPLC, according to the order of eluting peaks. [d] The major isomer was *S* (see the Supporting Information). [e] Conversion determined by ^{1}H NMR spectroscopy.

more sensitive than those catalysed by compound **1-Ag** towards structural changes on the substrates; whilst similar levels of enantioselectivity were obtained for compounds **4a** and **4b** with either catalyst (Table 1 and Table 2, entries 1 and 2), the TADDOL-derived catalyst showed higher selectivity for compounds **4c** and **4d** (Table 2, entries 3–6), thereby affording *ee* values of up to 73%. Conversely, changing the substitution pattern on the alkyl chain appears to have little effect: the reaction of the sterically demanding 2,2-diphenyl-substituted allenol to compound **4e** was much slower but gave similar level of enantioselectivity to that attained for compound **4b** (Table 2, entries 1, 2, 7, and 8). The formation of six-membered pyran **4f** also proceeded in high yield but was fairly unselective (Table 2, entries 9 and 10). In comparison, the cyclisation of β-allenoic acids into lactones **5a**–**5d** was facile but provided low enantioselectivities (Table 2, entries 11–18). In all cases, the hydroalkoxylation reactions produced optically active 1-alkenyl-substituted tetrahydrofurans **4b**–**4e** in good yields. In terms of stereoinduction, the formation of the same *S* enantiomer is favoured by both catalysts in the cyclisation of γ-allenols, whilst the opposite selectivity applies in the formation of lactones.

The cyclisation of γ-aminoallenes was also examined (Scheme 4, Table 3); on the whole, these reactions are slower than their corresponding O–H additions. For the cyclisation of compound **6a**, catalyst **2-Ag** is more active than catalyst **1-Ag**, although the latter catalyst is more selective (Table 3, entries 1 versus 12), furnishing an encouraging 64% *ee* for the *N*-tosyl-protected pyrrolidine (**7a**). Attributing the decreased reactivity to slow proton transfer, a selection of inorganic and organic bases was investigated as co-catalysts (see the Supporting Information, Table S2). For the reaction that is catalysed by compound **1-Ag**, inorganic bases, such as Cs_2CO_3, have an accelerative effect but destroy the selectivity (Table 3, entry 2). We postulate that this effect is due to the replacement of the chiral anion by a carbonate moiety, thereby forming a more-active, yet unselective, catalyst. On the other hand, no reaction occurred in the presence of a bulky non-nucleophilic base (Table 3, entry 3), thus suggesting that the reaction is inhibited by irreversible deprotonation. Eventually, pyridine was found to be the optimal additive, which accelerated the reaction significantly to afford the product (**7a**) in 68% *ee* (Table 3, entry 4).

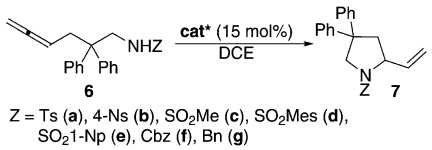

Scheme 4. Intramolecular N–H addition to allenes.

Table 3. Ag-catalysed hydroamination of aminoallenes.[a]

Entry	6/7	Cat.*	Additive[b]	*t* [h]	Conversion [%][c]	e.r.[d]
1	**6a/7a**	**1-Ag**	none	60	100	18:82
2	**6a/7a**	**1-Ag**	Cs_2CO_3	24	100	50:50
3	**6a/7a**	**1-Ag**	proton sponge[e]	24	–	–
4	**6a/7a**	**1-Ag**	pyridine	24	100	16:84
5	**6b/7b**	**1-Ag**	pyridine	24	60	43:57
6	**6c/7c**	**1-Ag**	pyridine	24	57	24:76
7	**6d/7d**	**1-Ag**	pyridine	24	38	30.5:69.5
8	**6e/7e**	**1-Ag**	pyridine	24	85	73:27
9	**6f/7f**	**1-Ag**	pyridine	24	84	76:24
10	**6f/7f**	**1-Ag**	none	24	76	75:25
11	**6g/7g**	**1-Ag**	pyridine	24	100	52.5:47.5
12	**6a/7a**	**2-Ag**	none	24	100	21.5:78.5
13	**6a/7a**	**2-Ag**	pyridine	24	4	37:63

[a] Reaction conditions: Compound **6a**–**6g** (0.1 mmol), catalyst, DCE, 0.5 mL, 23 °C. [b] 15 mol%. [c] Determined by ^{1}H NMR spectroscopy. [d] Determined by chiral HPLC, according to the order of eluting peaks. The major isomer was *S*, see reference [3d]. [e] 1,8-Bis(dimethylamino)-naphthalene.

However, the effect of the pyridine additive is not universal because it only has a marginal effect on the reaction of Cbz-derivative **6f** (Cbz = benzyloxycarbonyl; Table 3, entries 9 and 10), whilst the catalytic activity of compound **2-Ag** was inhibited by its presence (Table 3, entries 12 and 13). Thus, it appears that judicious matching between the base and substrate/catalyst is required. Notably, neither the level nor sense of stereoinduction (for compounds **7a** and **7f**) were affected by the presence of pyridine (Table 3, cf. entries 1 and 4 and entries 9 and 10), which supports the hypothesis that the stereodefining (C–N bond formation) and rate-limiting steps (protonolysis) operate independently of each other (Scheme 1).[5] The system appears to be fairly tolerant of different N-protecting groups, including sulfonamides, carbamates, and benzyl groups (Table 3, entries 4–11).[13] Comparing the reactivity of different sulfonamides (**6b**–**6e**), the electronic nature of the N-substituent appears to override steric effects: The use of a nosyl protecting group led to dramatic erosion in the reaction rate and selectivity (Table 3, entry 5), which were recovered with methane, mesitylene, and napthyl sulfonyl groups (Table 3, entries 6–8). Conversely, the reaction of the nucleophilic *N*-benzyl substrate (**6g**) was fast but unselective, whilst Cbz-protected **6f** afforded the second-highest selectivity in this series (Table 3, entries 9 and 10).

To delineate the origin(s) of the enantioselectivity, it is first necessary to ascertain the absolute configuration of the major isomers that are observed in the formation of compounds **4a** and **7c** (as representative compounds of the O–H and N–H addition reactions, respectively). The $[\alpha]_D$ values for compounds **4a** (−35°, 26% *ee*) and **7c** (−3.4°, 53% *ee*) are both levorotatory but differ widely in magnitude, which can be extrapolated to −134° and −6.4° for the pure enantiomers, respectively. Initially, the wavelength-dependent optical rotatory dispersion (ORD) spectra of these samples were recorded in $CHCl_3$; tetrahydrofuran **4a** displayed negative optical rotations across the whole wavelength range (275–800 nm, Figure 2a). In contrast, pyrrolidine **7a** displayed small negative optical rotations between 345–800 nm, which tuned into positive rotations at <345 nm (Figure 2b).

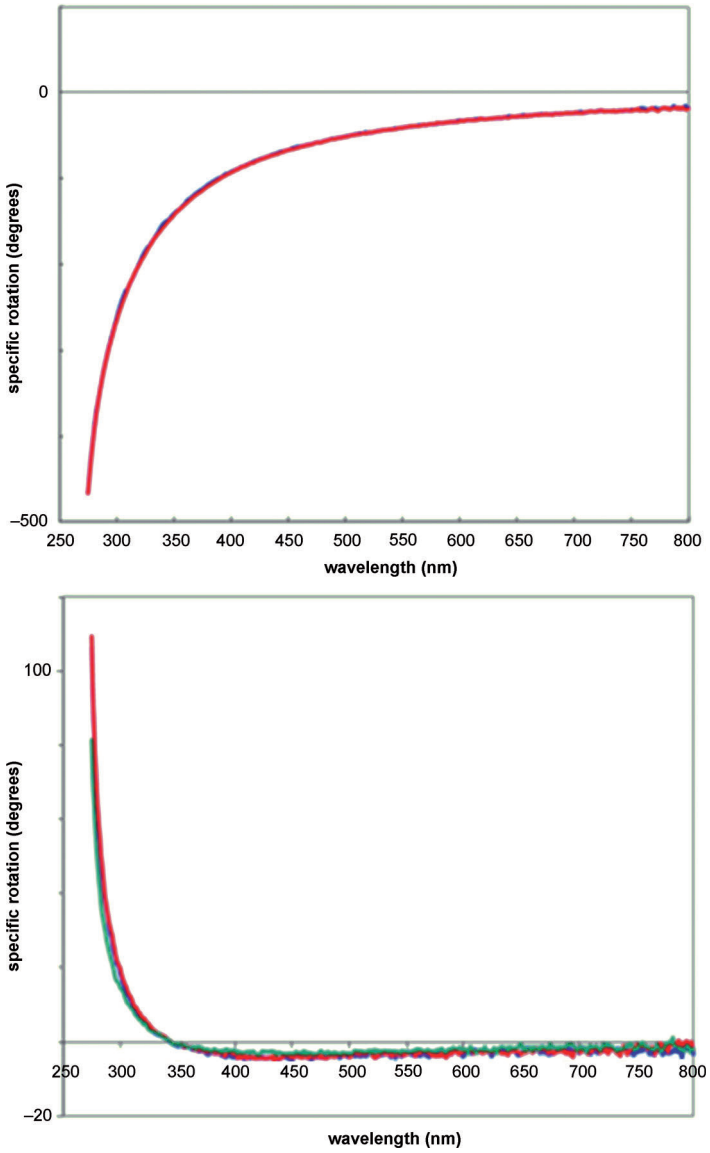

Figure 2. ORD spectra of compounds **4a** (top, 26% *ee*) and **7c** (bottom, 52% *ee*) in $CHCl_3$. Each measurement was repeated twice (red and green lines).

To help interpret this behaviour, conformational analysis was performed at the ωB97XD/6-311G(d,p) DFT level, including a continuum solvent correction (SCRF = CPCM). The DFT functional was selected[14] because it included the dispersion energy corrections that are now recognised as being key to successful conformational analysis; moreover, this functional has also been shown to reliably predict a range of chiroptical properties.[15] For compound **4a**, the calculations revealed at least four conformations within the range $\Delta G_{298} = 2\,\mathrm{kcal\,mol^{-1}}$ (see Web Table 1), with the lowest values separated by about $1.0\,\mathrm{kcal\,mol^{-1}}$ from the next two. The geometry of the lowest-energy conformation corresponded to the crystal structure that was reported for a closely related derivative.[16] Although the calculated $[\alpha]_{250-880}$ value for this conformation with an assigned *S* absolute configuration at the stereogenic centre was negative (see Web Table 1), the next two higher-energy conformations had positive rotations. The principle chromophore over this wavelength range is the gem-diphenyl group and the optical rotation clearly depends on the relative orientation of these two aryl rings, coupled to the conformation of the five-membered ring. Therefore, an unambiguous assignment of the absolute configuration would depend on a reliable identification of the dominant conformation and, whilst DFT calculations with included dispersion terms are probably reliable at this level, other evidence would be required to support these results.

Calculation of the electronic circular dichroism (ECD) spectra suggested that there would be no useful diagnostic features and so our attention turned to vibrational circular dichroism (VCD), which is still a relatively unexploited technique,[17] in part owing to the challenges in reliably predicting its features theoretically[18] and also to low sensitivity when enantiomerically pure (>98% *ee*) samples are not available, such as for compound **4a** (26% *ee*). To help improve the sensitivity of this technique, we focused on the region of C–H vibrations to exploit what might be termed the C–H anomeric effect, whereby an electronegative group X (X = O, N) that contains a lone pair can selectively weaken adjacent C–H bonds (Scheme 5). This effect helps

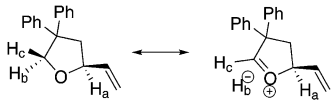

Scheme 5. Operation of the C–H anomeric effect.

to decrease the mixing of anomeric C–H stretching modes with any non-CH-anomeric groups present, thereby resulting in a localised mode at lower wavenumber; in this instance, an anomeric effect is observed for the three bonds ($C-H_a$, $C-H_b$, and $C-H_c$) that are adjacent to the stereogenic carbon atom of compound **4a** (for animations of these modes, see Web Table 1). The anomeric effect operates to a different extent for each of these three C–H groups, depending on their conformation. Thus, for conformation 2 of compound **4a**, the orientation of each C–H bond with respect to either of the two lone pairs on the adjacent oxygen atom (the positions of which were located as centroids of monosynaptic ELF basins[19]) controls the value of the C–H stretching wavenumber, the bond length, and the NBO-interaction energy between the lone-pair donor and the C–H* acceptor (Table 4).

Thus, a VCD spectrum that focuses on the anomeric C–H region should exhibit less ambiguity owing to conformational dependence than that predicted for the optical rotation. The calculated VCD spectra for conformations 1 and 2 of compound **4a** (for which opposite optical rotations had been predicted) show very similar and apparently clear-cut Cotton effects in ΔA for these anomeric C–H stretching modes (see the Supporting Information, Web Table 1). A

Table 4. Computed C–H anomeric effects in compound **4a**.[a]

C–H bond	ν [cm^{-1}]	θ [°][b]	C–H [Å]	NBO E2 energy [kcal mol^{-1}]
H_c	3015	157	1.0985	10.89
H_a	3070	113	1.0945	6.25
H_b	3129	85	1.0908	1.42

[a] See the Supporting Information, Web Table 1 for animations. [b] Angle between the C–H bond and the lone pair.

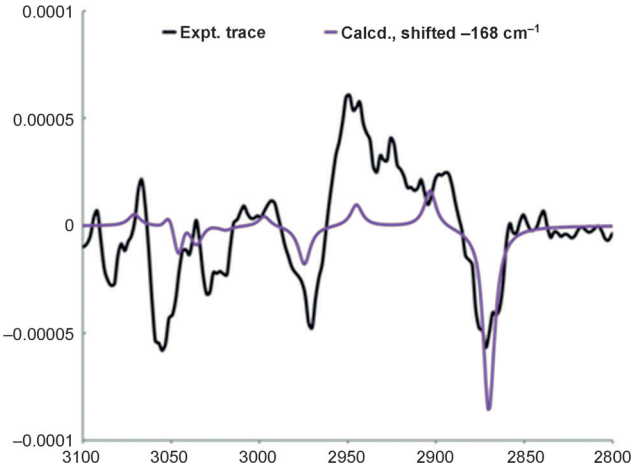

Figure 3. Observed (anharmonic, black) and calculated VCD spectra (harmonic, purple) in the C–H region for compound **4a**. The calculated spectrum was offset by 168 cm^{-1} to compensate for anharmonic effects.

comparison with the measured VCD spectrum in the C–H stretching region for compound **4a** (Figure 3) shows a better qualitative match over the five observed peaks for the *S* configuration than to the mirror-image spectrum of the *R* enantiomer. This result provides further supporting evidence for the assignment of the predominant enantiomer of compound **4a** as *S*.

Finally, the association of compound (*S*)-**4a**, as assigned by using chiroptical ORD and VCD methods, with an (enantiopure) rotation of −134° can be verified by literature data, based on synthetic transformations and the absolute configuration of a derivative by Flack analysis of the crystal structure.[3g,16,20]

For the nitrogen heterocycles, compound **7c** (52% *ee*) was chosen for assignment because it contains fewer atoms, thereby reducing the number of bond rotations and conformational complexity. The absolute configuration of compound **7f** has been previously determined by chemical transformation into a known compound.[3c] By comparison of the HPLC data, the assignment of an *S* configuration can be made. We assume that this assignment applies to all of the other major enantiomers that are produced by the Ag-catalysed reactions.

However, the stereochemical assignment for compound **7c** is more challenging than for compound **4a**. There are still at least four conformations that are predicted to be spanned by as little as $\Delta G_{298} = 0.2$ kcal mol^{-1} (see Web Table 1) and so it is more than likely that the measurements will be made on a mixture of multiple conformers. The predicted optical rotations for all of the conformations of the *S* configuration are positive over the entire wavelength range, which agrees with the measured ORD below 350 nm, but the assignment becomes less clear-cut at higher wavelengths, where the measured rotation is very small. For the vibrational C–H spectrum, nitrogen (X=N) is a weaker electron donor than oxygen and hence, the induced C–H anomeric effect would be expected to be smaller. Moreover, multiply populated conformations significantly lower the signal-to-noise ratio for a given concentration because the signal is distributed amongst more peaks. Indeed, the measured VCD spectrum for compound **7c** shows a very much-weaker signal than for compound **4a**, despite the higher *ee* value of the sample. Whilst there is a perceptibly better match to that predicted for the *S* configuration (Figure 4), the confidence level of assignment as (*S*)-**7c** is lower than that for compound **4a**.

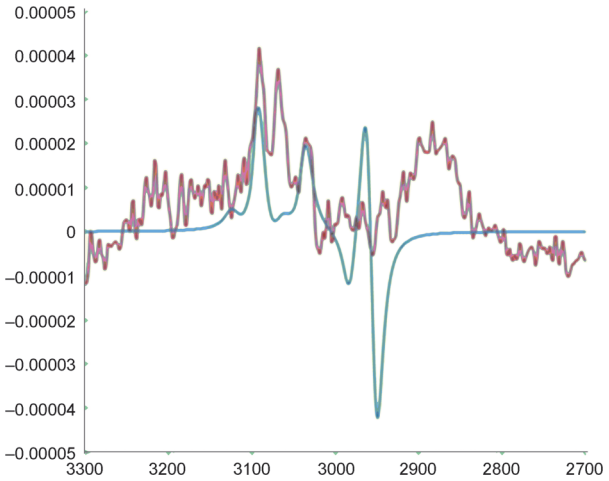

Figure 4. Measured (red) and calculated VCD spectra (blue) for compound **7c**.

One of the most-intriguing aspects of these reactions is the level of enantioselectivity that can be achieved with compound **1-H**, which contains relatively few steric/chiral elements. We have previously modelled the transition state for the cyclisation of γ-allenols with achiral counteranions.[5] In addition to including the chiral anion, we also incorporated some changes to the computational procedure. As before, the basis set was cc-VDZ on all elements except Ag, which was aug-cc-pVDZ-pp. The functional was changed to ωB97XD, which has been shown to reproduce reaction barriers well and which also accounts for dispersion interactions.[21] Moreover, the effect of solvent by using a continuum model is now included in the modelling.

For the formation of both compounds **4a** and **7c**, two diastereomeric transition states were located that corresponded to both the *R* and *S* enantiomers in the presence of the chiral anion (*1R,3S,5S,7R*)-tetramethyl-2,4,6-trioxa-8-phos-

phatricyclo[3.3.1.13.7]decan-8-ol-8-oxide[8] (for transition-state 3D model coordinates and animations of the normal reaction modes, see Web Table 2). The calculated discrimination for compound **4a** (0.2 kcal mol^{-1}) favours the assignment (*R*)-**4a**, but such a small magnitude merely confirms that the reaction proceeds with a low *ee* value. The discrimination for compound (*S*)-**7c** was rather more significant (0.70 kcal mol^{-1}), which corresponds to 54% *ee*, similar to that found experimentally. This result is further evidence, albeit only indirect, in favour of the assignment of (*S*)-**7c** as the major enantiomer.

With the enantiomers assigned, it is now possible to comment on the stereochemistry of the catalyst system. Previously, the absolute stereoinduction of gold-catalysed systems was dependent upon the nature of the nucleophile, rather than on the source of chirality or on the degree of substitution on the allene; that is, by using either a chiral diphosphine ligand or a chiral counteranion, opposite enantiomers were preferred for O–H and N–H addition reactions.[3a,d] In contrast, these silver catalysts favour the same sense of stereoinduction (*S*) in both the hydroalkoxylation and hydroamination reactions (Table 1, entries 1, 2, 5, and 6 and Table 3, entries 9 and 10). On the other hand, for certain reactions, such as the formation of pyran **4f** and lactones **5a**–**5d**, opposite enantioselectivities were observed with compounds **1-Ag** and **2-Ag**, thus indicating a synergistic relationship between the catalyst and the substrate.

From the chemist's point of view, the origin of the enantiomeric excess has to be traced back to preferable interactions in the formation of one of the enantiomers to the detriment of the other. More specifically, following transition-state theory, other procedures should be evaluated to help identify the factors that lead to differential stabilization of the diastereomeric transition-state complexes. This stabilization turns out to be a delicate balance of numerous weak noncovalent interactions; a balance that can be very difficult to achieve by using DFT calculations based on free energies that were derived from covalent terms (i.e., normal vibrational modes). Recently, it has been shown that, although the energetic balance of weak interactions is cumbersome to establish from energetics alone, the (electron) density reconstruction by using these methods is accurate enough to reveal the interactions that are present in the system.[22] This principle is behind the recently reported index for detecting noncovalent interactions (NCIs; for more technical details on the method, see Supporting Information).[22] This index enables the identification and characterisation of weak interactions of various strengths as chemically intuitive isosurfaces that reveal both stabilizing (hydrogen-bonding interactions in blue, van der Waals interactions in green) and destabilizing interactions (steric clashes in red).[23]

By depicting NCIs for the most-stable conformers of the (*R/S*)-**4a-Ag-H-1** and (*R/S*)-**7c-Ag-H-1** diastereomeric transition states that were located by DFT methodology (see Web Table 2), important chemical features can be identified that explain the stability of the complex of compound (*S*)-**7c** (Figure 5 and Table 5). Immediately obvious is the role

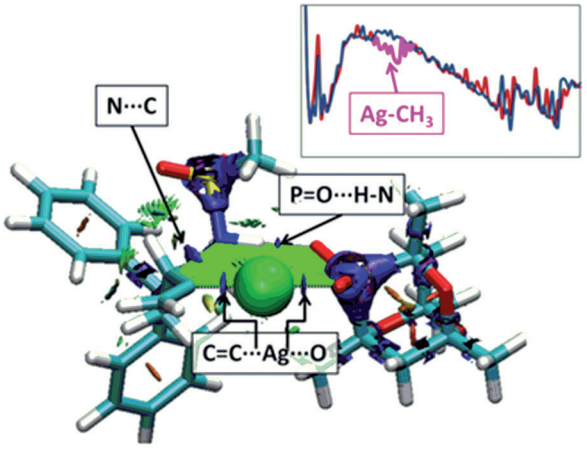

Figure 5. NCI reduced-gradient isosurfaces for the transition state that involves compound (*S*)-**7c**; the colour coding is graded over the range blue = attractive, green = weakly attractive, yellow = weakly repulsive, and red = strongly repulsive. The most-relevant interactions for the stability of the transition state are highlighted. The inset shows the difference between these noncovalent interactions for the *R* and the *S* enantiomers in the s(ρ) space, which can be associated to the Ag–CH_3 interactions.

Table 5. Energy differences between the (*R/S*)-**4a**-**Ag-H-1** and (*R/S*)-**7c**-**Ag-H-1** transition states.[a]

System	ΔG_{298} [kcal mol^{-1}]	Digital repository identifier
(*R*)-**4a**	0.0	10042/to-8399
(*S*)-**4a**	0.2	10042/to-9255
(*R*)-**7c**	0.0	10042/to-8503
(*S*)-**7c**	−0.70	10042/to-9256

[a] See Web Table 2 for animated transition states.

of dispersion interactions (green) in the stabilization of the complex: the bond-formation and bond-rupture process is at its highest peak and multiple van der Waals interactions are observed (for example, see the interactions between the Ph rings). A clear example of steric repulsion can be found inside the anionic ligand, where the cage is known to give rise to an important steric clash. However, these interactions are located within each reactant and they are expected not to suffer many changes along the reaction; thus they should not have a big influence on the kinetics and the enantioselectivity. In this sense, it is more interesting to look at the interactions that link the anionic ligand and the substrate (Figure 5, highlighted). Firstly, the interaction between the catalysing Ag cation and the reactants clearly appears as two blue regions between them. A stabilizing X–C interaction also appears that is being broken in step 1 of the reaction (Scheme 1). Finally, an important hydrogen bond is found between P=O and H-X (X = O, N). These interactions in both complexes **4a** and **7c** form a closed cycle that is behind the stability of the transition states (indicated as green plane in Figure 5).

The enantiomeric effects are subtle and the small differences that are revealed by transition energies alone (Table 5) are not able to discriminate between the different enantiomers to determine which is more favoured (for other

figures, see the Supporting Information). To have a more-quantitative look at the interactions that stabilise the complexes, it is useful to compare their NCI profiles in terms of the density. When we compare the plots for the **7c-Ag-H-1** complex, a new peak appears in the *S* enantiomer that is not present in the *R* enantiomer (Figure 5, inset, pink arrow), which identifies an enhanced interaction at the C=CH_2 enantiomeric source. When the corresponding **4a-Ag-H-1** complexes are compared, a similar feature is found in the *S* enantiomer. Although in this case it is not as clear in the 2D plot, it does indeed project us to the same part of molecular space (see the Supporting Information, Figures S17 and S18). In other words, NCI analysis is able to highlight the differential interactions that explain the (*S*) enantiomeric excess, where the comparison of energy differences is ambiguous.

The formation of this interaction is facilitated by the protocycle around the Ag^+ cation in the transition state, mediated by the X proton donors (X = O and N). This observation explains the fact that both X atoms promote the same enantiomer. Moreover, this is a purely quantum effect, because the distances remain the same in both conformers. Only the density is able to distinguish between the *R* and *S* configurations.

Finally, interestingly, the NCI features extend beyond the plane of interaction: they spread to the O-P-O part of the anion and to the N-substituent in complex **7c**. This "cooperative" interaction explains their ability to tune the enantioselectivity. We feel that the procedure outlined herein is a general one for establishing the regions of a molecule that are primarily responsible for transition-state diastereoselectivity, which will be the target of our future work.

Conclusion

This work demonstrates, for the first time, that chiral silver complexes can be used to facilitate the addition of O–H and N–H bonds to C=C bonds with significant levels of enantioselectivity. Encouraging ee values of up to 73% and 68% can be achieved for the addition of O–H and N–H groups, respectively. Although the stereoselectivity is modest at present, the combination of silver with a chiral counteranion is a new catalyst system for this type of asymmetric catalysis, which justifies further research in this area.

We also applied new theoretical methods to uncover several important aspects regarding the stereochemistry of the reaction, including the assignment of absolute configurations based on C–H anomeric effects in the VCD spectra and the delineation of stereoselectivity through free-energy differences and subtle noncovalent interactions in the computed transition states for the reactions. This study highlights the significance of weak effects on reaction selectivity, which is often overlooked in asymmetric synthesis.[24] Further development and exploitation of this NCI method has the potential to deliver unique semi-quantitative insight into the origins of catalytic stereoselectivity.

Experimental Section

Synthesis of 1-Ag (method 1): Ag_2CO_3 (0.5 equiv) was added in a single portion to a solution of **1-H**[8,25] (1 equiv) in EtOH (5 mL). The resulting mixture was protected from light and stirred vigorously overnight. The mixture was centrifuged and the solvent was decanted. A further portion of EtOH (5 mL) was added to the remaining solid and the mixture was centrifuged and decanted again. The organic extracts were combined and concentrated under vacuum. The resulting silver salt was dried overnight in vacuo. Compound **1-Ag** was obtained as a fluffy white solid (96%). M.p. > 300 °C (dec.); $[\alpha]_D^{25} = +39.0°$ ($c = 0.5$, $CHCl_3$); ^{1}H NMR (400 MHz, $CDCl_3$, 25 °C): $\delta = 2.43$ (dd, $J = 13.2$, 1.9 Hz, 2H), 1.96 (dd, $J = 23.6$, 13.2 Hz, 2H), 1.43 (s, 6H), 1.34 ppm (6H, d, $J = 11.5$ Hz); ^{13}C NMR (100 MHz, $CDCl_3$, 25 °C): $\delta = 96.5$, 72.2, 71.2, 43.4, 27.2, 18.9 ppm; ^{31}P NMR (162 MHz, $CDCl_3$, 25 °C): $\delta = 31.0$ ppm (br s); IR: $\tilde{\nu} = 3001$, 2921, 1638, 1451, 1378, 1343, 1202, 1136, 1087, 1023, 977, 890, 678 cm^{-1}; MS (FAB): *m/z* (%): 1527 (40) $[(M)_4Ag_5]^+$, 1173 (89) $[(M)_3Ag_4]^+$, 355 (15) $[(M)Ag]^+$; elemental analysis calcd (%) for $C_{10}H_{16}AgO_5P$: C 33.83, H 4.54; found: C 34.01, H 4.54.

Synthesis of 2-Ag (method 2): Ag_2CO_3 (0.5 equiv) was added in a single portion to a solution of **2-H**[10] (1 equiv) in CH_2Cl_2 (5 mL) followed by H_2O (5 mL). The resulting mixture was protected from light and stirred vigorously for 2 h. After this time, the mixture was diluted with CH_2Cl_2 (10 mL) and H_2O (10 mL). The biphasic suspension were separated and the aqueous layer was extracted with further portions of CH_2Cl_2 (2× 15 mL). The combined organic extracts were filtered through celite and concentrated under vacuum. The resulting silver salt was dried overnight in vacuo. Compound **2-Ag** was obtained as a fluffy white solid (92%). M.p. > 234 °C (decomp); $[\alpha]_D^{25} = -219.0°$ ($c = 1.0$, $CHCl_3$); ^{1}H NMR (400 MHz, $CDCl_3$, 25 °C): $\delta = 7.61$ (d, $J = 7.6$ Hz, 4H), 7.52 (d, $J = 7.6$ Hz, 4H), 7.37–7.06 (m, 12H), 5.18 (s, 2H), 0.82 ppm (s, 6H); ^{13}C NMR (100 MHz, $CDCl_3$, 25 °C): $\delta = 143.5$, 139.6 (d, $J = 9.2$ Hz), 128.8, 128.2, 128.1, 127.6, 127.2, 126.9, 113.7, 87.9 (d, $J = 7.0$ Hz), 79.4, 26.5 ppm; ^{31}P NMR (162 MHz, $CDCl_3$, 25 °C): $\delta = -0.15$ ppm (br s); IR: $\tilde{\nu} = 3057$, 2991, 2344, 1493, 1447, 1210, 1051, 1036, 897, 740, 967 cm^{-1}; MS (FAB): *m/z* (%): 635 (31) $[M]^+$, 431 (45), 179 (100); elemental analysis calcd (%) for $C_{31}H_{28}AgO_6P$: C 58.60, H 4.44; found: C 58.45, H 4.36.

Typical procedure for the Ag-catalysed reactions: A screw-capped vial was charged with a magnetic stirrer bar, compound **1-Ag** or **2-Ag** (5 or 15 mol%), the requisite substrate (0.1 mmol), and an additive (if used, 0.1 mmol). 1,2-Dichloroethane (DCE, 0.5 mL) was added and the mixture was stirred at RT in the dark. Conversions were monitored by ^{1}H NMR spectroscopy. Upon completion, the solvent was evaporated and the product was purified by column chromatography on silica gel.

Acknowledgements

We thank the EPSRC for studentship support (J.L.A.). We thank the Ministerio de Educación Español, the Xunta Galicia (Angeles Alvariño program), and the Fundación Barrié de la Maza for postdoctoral fellowships to J.C.G., L.A.A., and E.M.B., respectively. We thank Professor Widenhoefer (Duke University) for providing the HPLC conditions for compound **4a** and Professor Mikami (Tokyo Institute of Technology) for clarification on the stereochemical assignment of compound **4a**.

[1] a) V. M. Arredondo, F. E. McDonald, T. J. Marks, *Organometallics* **1999**, *18*, 1949–1960; b) R. W. Bates, V. Satcharoen, *Chem. Soc. Rev.* **2002**, *31*, 12–21; c) X. H. Yu, S. Seo, T. J. Marks, *J. Am. Chem. Soc.* **2007**, *129*, 7244–7245; d) T. Bai, S. M. Ma, G. C. Jia, *Coord. Chem. Rev.* **2009**, *253*, 423–448; e) C. J. Weiss, T. J. Marks, *Dalton Trans.* **2010**, *39*, 6576–6588.

[2] The enantioselective hydroamination of aminoallenes was first achieved by using a titanium catalyst of chiral amino alcohols and, very recently, by using sulfonamide–alcohol complexes (including tantalum). However, only up to 16% *ee* has been achieved: a) J. M.

Hoover, J. R. Petersen, J. H. Pikul, A. R. Johnson, *Organometallics* **2004**, *23*, 4614–4620; b) A. J. Hickman, L. D. Hughs, C. M. Jones, H. Li, J. E. Redford, S. J. Sobelman, J. A. Kouzelos, A. R. Johnson, *Tetrahedron: Asymmetry* **2009**, *20*, 1279–1285; c) K. E. Near, B. M. Chapin, D. C. McAnnally-Linz, A. R. Johnson, *J. Organomet. Chem.* **2011**, *696*, 81–86.

[3] a) G. L. Hamilton, E. J. Kang, M. Mba, F. D. Toste, *Science* **2007**, *317*, 496–499; b) R. L. LaLonde, B. D. Sherry, E. J. Kang, F. D. Toste, *J. Am. Chem. Soc.* **2007**, *129*, 2452–2453; c) Z. Zhang, C. F. Bender, R. A. Widenhoefer, *J. Am. Chem. Soc.* **2007**, *129*, 14148–14149; d) Z. B. Zhang, C. F. Bender, R. A. Widenhoefer, *Org. Lett.* **2007**, *9*, 2887–2889; e) Z. B. Zhang, R. A. Widenhoefer, *Angew. Chem.* **2007**, *119*, 287–289; *Angew. Chem. Int. Ed.* **2007**, *46*, 283–285; f) K. Aikawa, M. Kojima, K. Mikami, *Angew. Chem.* **2009**, *121*, 6189–6193; *Angew. Chem. Int. Ed.* **2009**, *48*, 6073–6077; g) K. Aikawa, M. Kojima, K. Mikami, *Adv. Synth. Catal.* **2010**, *352*, 3131–3135; h) R. L. LaLonde, Z. J. Wang, M. Mba, A. D. Lackner, F. D. Toste, *Angew. Chem.* **2010**, *122*, 608–611; *Angew. Chem. Int. Ed.* **2010**, *49*, 598–601; i) H. Li, S. Du Lee, R. A. Widenhoefer, *J. Organomet. Chem.* **2011**, *696*, 316–320.

[4] a) N. D. Shapiro, V. Rauniyar, G. L. Hamilton, J. Wu, F. D. Toste, *Nature* **2011**, *470*, 245–249; b) L. Ackermann, A. Althammer, *Synlett* **2008**, 995–998.

[5] J. L. Arbour, H. S. Rzepa, A. J. P. White, K. K. Hii, *Chem. Commun.* **2009**, 7125–7127.

[6] The axis-to-centre transfer of chirality from optically active precursors to the products has previously been achieved by using silver catalysis, see: a) D. Lathbury, T. Gallagher, *J. Chem. Soc. Chem. Commun.* **1986**, 114–115; b) N. J. S. Huby, R. G. Kinsman, D. Lathbury, P. G. Vernon, T. Gallagher, *J. Chem. Soc. Perkin Trans. 1* **1991**, 145–155.

[7] For the recent use of chiral silver–phosphate complexes for the kinetic resolution of racemic allenic alcohols, see: Y. Wang, K. Zheng, R. Hong, *J. Am. Chem. Soc.* **2012**, *134*, 4096–4099.

[8] J. Hopewell, P. Jankowski, C. L. McMullin, A. G. Orpen, P. G. Pringle, *Chem. Commun.* **2010**, *46*, 100–102.

[9] Compound **1-H** was kindly provided by Professor Paul G. Pringle (the University of Bristol, U.K.).

[10] A. Voituriez, A. B. Charette, *Adv. Synth. Catal.* **2006**, *348*, 2363–2370.

[11] J. G. Taylor, L. A. Adrio, K. K. Hii, *Dalton Trans.* **2010**, *39*, 1171–1175.

[12] Triflic acid catalyses the cyclisation of compound **4a** in a 6-*endo* manner, see: K. Mori, S. Sueoka, T. Akiyama, *Chem. Lett.* **2009**, *38*, 628–629.

[13] So far, gold-catalysed reactions have only been reported with certain sulfonamides, carbamates, and ureas.

[14] J.-D. Chai, M. Head-Gordon, *Phys. Chem. Chem. Phys.* **2008**, *10*, 6615–6620.

[15] F. Cherblanc, Y. P. Lo, E. De Gussem, L. Alcazar-Fuoli, E. Bignell, Y. He, N. Chapman-Rothe, P. Bultinck, W. A. Herrebout, R. Brown, H. S. Rzepa, M. J. Fuchter, *Chem. Eur. J.* **2011**, *17*, 11868–11875.

[16] Y. K. Chung, G. C. Fu, *Angew. Chem.* **2009**, *121*, 2259–2261; *Angew. Chem. Int. Ed.* **2009**, *48*, 2225–2227.

[17] For a review, see L. A. Nafie, *Nat. Prod. Commun.* **2008**, *3*, 451–466.

[18] V. P. Nicu, E. J. Baerends, *Phys. Chem. Chem. Phys.* **2009**, *11*, 6107–6118.

[19] C. S. M. Allan, H. S. Rzepa, *J. Chem. Theory Comput.* **2008**, *4*, 1841–1848.

[20] The absolute stereochemical assignments as reported in reference [3g] have since been reassigned: K. Aikawa, M. Kojima, K. Mikami, *Adv. Synth. Catal.* **2011**, *353*, 2882.

[21] H. S. Rzepa, *Chem. Commun.* **2011**, *47*, 1851–1853.

[22] E. R. Johnson, S. Keinan, P. Mori-Sánchez, J. Contreras-García, A. J. Cohen, W. Yang, *J. Am. Chem. Soc.* **2010**, *132*, 6498–6506.

[23] J. Contreras-García, W. Yang, E. R. Johnson, *J. Phys. Chem. A* **2011**, *115*, 12983–12990.

[24] Also see: A. M. R. Smith, H. S. Rzepa, A. J. P. White, D. Billen, K. K. Hii, *J. Org. Chem.* **2010**, *75*, 3085–3096.

[25] J. H. Downing, J. Floure, K. Heslop, M. F. Haddow, J. Hopewell, M. Lusi, H. Phetmung, A. G. Orpen, P. G. Pringle, R. I. Pugh, D. Zambrano-Williams, *Organometallics* **2008**, *27*, 3216–3224.

Received: February 19, 2012
Revised: April 12, 2012
Published online: ■■ ▮▮, 0000

Come on allene: The enantioselective addition of O–H and N–H bonds to allenes was achieved by using chiral silver complexes. A new computational method revealed that the stereoselectivity resulted from weak noncovalent interactions.

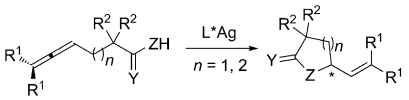

hydroalkoxylation, Y = Ph_2, H_2; Z = O
hydroacylalkoxylation, Y = Z = O
hydroamination, Y = Ph; Z = NP (P = protecting group)

Asymmetric Catalysis

J. L. Arbour, H. S. Rzepa, J. Contreras-García, L. A. Adrio, E. M. Barreiro, K. K. Hii* . .* ▮▮▮▮–▮▮▮▮

Silver-Catalysed Enantioselective Addition of O–H and N–H Bonds to Allenes: A New Model for Stereoselectivity Based on Noncovalent Interactions